Food chain chaos with canard explosion

Bo Deng[a)]
Department of Mathematics, University of Nebraska–Lincoln, Lincoln, Nebraska 68588

(Received 17 February 2004; accepted 29 August 2004; published online 16 November 2004)

The "tea-cup" attractor of a classical prey–predator–superpredator food chain model is studied analytically. Under the assumption that each species has its own time scale, ranging from fast for the prey to intermediate for the predator and to slow for the superpredator, the model is transformed into a singular perturbed system. It is demonstrated that the singular limit of the attractor contains a canard singularity. Singular return maps are constructed for which some subdynamics are shown to be equivalent to chaotic shift maps. Parameter regions in which the described chaotic dynamics exist are explicitly given. © *2004 American Institute of Physics*. [DOI: 10.1063/1.1814191]

The ecosystem is a web of predator–prey food chains. Studying how complex dynamics arise from food chains is without doubt critical to any attempt to understand ecocomplexity. This paper is the last in a series of four papers devoted to categorizing and analyzing chaos generating mechanisms for the Rosenzweig–MacArthur food chain model.

I. INTRODUCTION

Chaotic population dynamics was first discovered in the mid-1970s from the classical logistic map.[1] Chaos for continuous ecological models was discoverd soon after.[2,3] Attractors of these early types can be classified as the type of Rössler's attractor.[4] A second generation of food chain chaos was discovered by Hastings[5] more than a decade later. Another type containing Shilnikov's homoclinic saddle-focus orbit[6] was found by McCann and Yodzis.[7] All these discoveries were made numerically from mathematical models. Hastings' attractor looks like a "tea-cup" and it has been figuratively referred to as such in the literature.[8,7,9]

A geometric model was proposed for the tea-cup attractor by Kuznetsov and Rinaldi in Ref. 9. The two authors treated the food chain model under the assumption that the top-predator's population is slowing varying. When the top-predator variable is frozen as a parameter, the system can be viewed as a family of two-dimensional predator–prey systems parametrized by the top-predator density. They demonstrated that this one-parameter family of systems undergoes a supercritical Hopf bifurcation at some top-predator density, see Fig. 1(a). The Hopf bifurcation gives rise to a family of predator–prey periodic cycles for all top-predator densities below the bifurcation point and a family of stable equilibrium states over a finite range above the bifurcation point. The parametrized cycles form a paraboloid-shaped surface whose vertex is at the bifurcation point, and the stable equilibrium states form a curve from the vertex at one end and go through a saddle-node bifurcation at the higher end of the top-predator density range. The unstable equilibrium branch from the saddle-node point folds backward and reinjects itself back to the paraboloid surface. In this way a tea-cup is formed with the periodic branch from the Hopf bifurcation being the cup and the equilibrium branch being part of the handle. The tea-cup attractor can then be envisioned by following a typical orbit of the system when the singular parameter, which represents the slow reproduction rate of the top-predator is made to be small. In fact one can arrange the top-predator's nullcline in such a way so that for the relaxed full system such an orbit winds around the periodic surface in the predator–prey directions and at the same time slowly drifts in the increasing direction of the top predator. In a finite time the orbit reaches the cup's base and tightly hugs the stable equilibrium branch until it falls off the fold point at which the density of the top-predator is high enough to cause the predator density to collapse. This sends the orbit to the decreasing side of top-predator's nullcline with low predator density. As a result the orbit drifts down in both the predator and the top-predator's densities until the latter becomes low enough to allow the predator to recover. At the predator's recovery point the orbit goes up in the predator direction and reconnects the predator–prey cycle surface again. At this point the whole process starts anew, giving rise to the wondering feature of the attractor. In this way Kuznetsov and Rinaldi obtained a good qualitative description of the attractor. However the authors did not show why their geometric prototype must lead to chaotic dynamics or to periodic cycles.

The paper is organized as follows. We start with some preliminary properties of the model and introduce the parameter region under consideration in Sec. II. We then review the theory of canard explosion and the theory of Pontryagin's delay of loss of stability in Sec. III that are essential for the construction of the singular Poincaré return maps in Sec. IV. The return maps are constructed, analyzed in Sec. IV. Closing remarks are given in the last section. A technical result is proved in the Appendix.

II. PRELIMINARY ANALYSIS

We continue to consider the following Rosenzweig–MacArthur model[10] for food chains analyzed in Refs. 5, 7, 9, and 11–15:

[a)]Electronic mail: bdeng@math.unl.edu

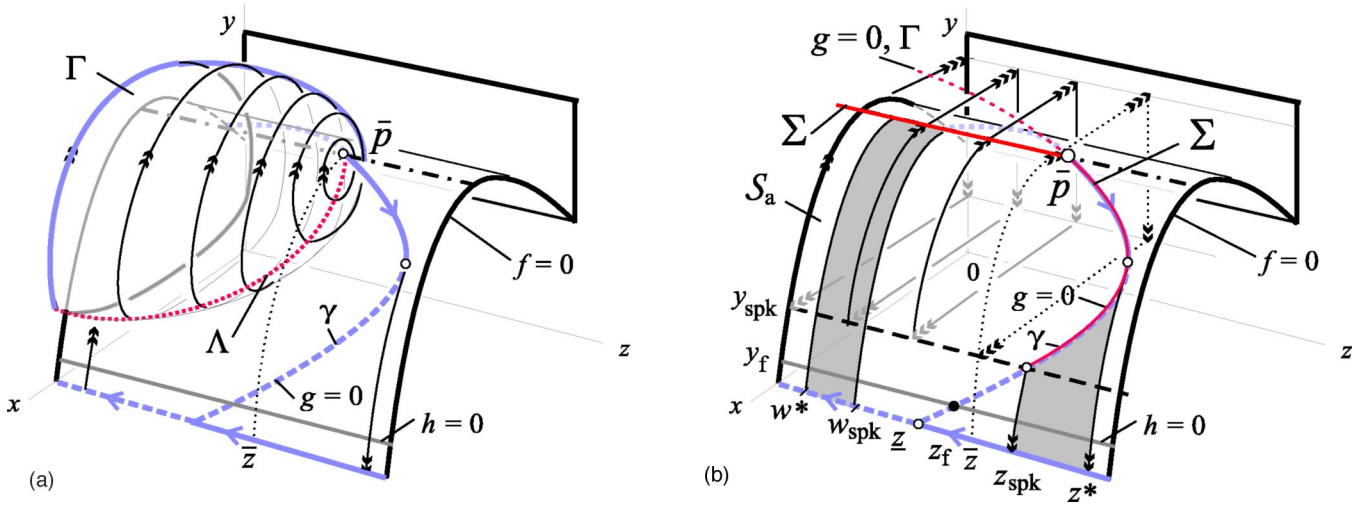

FIG. 1. (Color online). Nullcline surfaces and bifurcation surfaces when z is fixed as a parameter ($\varepsilon=0$). (a) The perturbed case, $0<\zeta\ll 1$. (b) The limiting case, $\zeta=0$. (a) Point $\bar{p}=\bar{p}(\zeta)$ is a Hopf bifurcation point and the paraboloidlike surface is the corresponding bifurcation branch for periodic orbits. (b) Point $\bar{p}$ is the canard point, which is the limiting point of the Hopf bifurcation point when $\zeta\to 0$. Oriented lines are singular orbits at the limit $\zeta=\varepsilon=0$. The periodic bifurcation surface of (a) is torn wide open at the canard point $\bar{p}$ at the limit $\zeta=0$, the canard explosion phenomenon. The curve Λ is the intersection of the canard-Hopf periodic surface with the attracting part of the x-nullcline $\mathcal{S}_a$.

$$\dot{x}=x\left(r-\frac{rx}{K}-\frac{p_1y}{H_1+x}\right),$$

$$\dot{y}=y\left(\frac{c_1x}{H_1+x}-d_1-\frac{p_2z}{H_2+y}\right), \tag{2.1}$$

$$\dot{z}=z\left(\frac{c_2y}{H_2+y}-d_2\right),$$

for a logistic prey (x), a Holling type II predator (y), and a Holling type II top predator (z).[16] With the following changes of variables and parameters,

$$t\to c_1t,\ \ x\to\frac{1}{K}x,\ \ y\to\frac{p_1}{rK}y,\ \ z\to\frac{p_2p_1}{c_1rK}z,$$

$$\zeta=\frac{c_1}{r},\ \ \varepsilon=\frac{c_2}{c_1},\ \ \beta_1=\frac{H_1}{K},\ \ \beta_2=\frac{H_2}{Y_0}\ \text{ with } Y_0=\frac{rK}{p_1}, \tag{2.2}$$

$$\delta_1=\frac{d_1}{c_1},\ \ \delta_2=\frac{d_2}{c_2},$$

which were first used in Ref. 13 and subsequently in Refs. 14 and 15, Eqs. (2.1) are changed to the following dimensionless form:

$$\zeta\dot{x}=x\left(1-x-\frac{y}{\beta_1+x}\right):=xf(x,y),$$

$$\dot{y}=y\left(\frac{x}{\beta_1+x}-\delta_1-\frac{z}{\beta_2+y}\right):=yg(x,y,z), \tag{2.3}$$

$$\dot{z}=\varepsilon z\left(\frac{y}{\beta_2+y}-\delta_2\right):=\varepsilon zh(y).$$

Under the drastic trophic time diversification hypothesis[12,13] that the *maximum per-capita growth rate decreases from bottom to top along the food chain*, namely

$$r\gg c_1\gg c_2>0\ \text{ or equivalently } 0<\zeta\ll 1$$

and $0<\varepsilon\ll 1$,

Eq. (2.3) becomes a singularly perturbed system of three time scales, with the rates of change for the dimensionless prey, predator, and top predator ranging from fast to intermediate to slow, respectively.

Geometric theory of singular perturbation thus is readily applicable to Eq. (2.3). In particular, nullcline analysis will be used extensively throughout. Nullclines are surfaces along which one of the derivatives is 0. The x-nullcline ($\dot{x}=0$) consists of two smooth surfaces: the trivial branch $x=0$, and the nontrivial branch $\mathcal{S}:=\{f(x,y)=0\}$ on which we can solve for y as a quadratic function $y=\phi(x)=(1-x)(\beta_1+x)$. The graph of the nontrivial branch is the cylindrical parabola shown in Fig. 1. The fold of $\mathcal{S}$ is given by $(\bar{x},\bar{y})$, also the maximum point of $y=\phi(x)$, where $\bar{x}=(1-\beta_1)/2$, $\bar{y}=(1+\beta_1)^2/4$. It divides $\mathcal{S}$ into two parts: $\mathcal{S}_a:=\{f=0, f_x<0\}$ and $\mathcal{S}_r:=\{f=0, f_x>0\}$, consisting of, respectively, attracting and repelling equilibrium points for the x equation. The trivial and nontrivial x-nullclines meet along the line $\mathcal{S}_r\cap\{x=0\}=\{x=0, y=y_{\rm trn}\}$, $y_{\rm trn}=\beta_1$, consisting of transcritical points which are double zero points for $\dot{x}$.

Similarly, the y-nullcline ($\dot{y}=0$) consists of two surfaces: the trivial one, $y=0$, and the nontrivial one $g(x,y,z)=0$ (not shown here but in Refs. 13–15). The intersection, denoted by γ, of $g=0$ and $f=0$ is a curve on the cylindrical parabola $\mathcal{S}$, see Fig. 1(b). A few points on γ are essential for our construction later. First, by definition, any intersection of the cylindrical parabola fold $\{x=\bar{x}, y=\bar{y}\}$ with the y-nullcline is a canard point. Our system has a unique canard denoted by $\bar{p}=(\bar{x},\bar{y},\bar{z})=\gamma\cap\{x=\bar{x}, y=\bar{y}\}$. More discussions will follow in

the subsequent sections on canard points. Second, under the conditions that

$$\bar{x} = \frac{1-\beta_1}{2} < \frac{\beta_1\delta_1}{1-\delta_1} = x_*$$

and

$$\beta_2 < \frac{(\beta_1+1)^3}{\beta_1}\left(\frac{1}{\beta_1+1} - \delta_1\right),$$

the curve γ must develop a unique fold point $p^* = (x^*, y^*, z^*)$ over the interval $0 < y^* < \bar{y}$ at which z is maximal along γ (see Proposition 6.1). Last, the intersection of the trivial y-nullcline with the nontrivial y-nullcline on the cylindrical parabola $f(x,y)=0$ at $\underline{p} = (\underline{x}, \underline{y}, \underline{z}) = (1, 0, \beta_2(1/(\beta_1+1) - \delta_1))$ is the transcritical point for the y equation on the cylindrical parabola. As we will demonstrate below, it is because of the canard that the attractor has a cup, the y-fold as the handle, and the y-transcritical point as the chaos.

The z-nullcline consists of the trivial nullcline $z=0$ and the nontrivial one $h(y)=0$, which is a plane $y=y_f=\beta_2\delta_2/(1-\delta_2)$ parallel to the xz plane. The intersection of the three nontrivial nullclines gives the unique nontrivial equilibrium point, $p_f(x_f, y_f, z_f) = \{y=y_f\} \cap \gamma$. This point is stable if and only if it lies on the solid part of γ between the canard point $\bar{p}$ and the y-fold point p^*.

Similarly defined as in Refs. 13 and 15, let $y_{\text{spk}}(z)$ be the value of Pontryagin's delay of loss of stability (PDLS), see Refs. 11, 13, 15, and 17–19, determined by the integral

$$\int_{y_{\text{spk}}}^{\bar{y}} \frac{f(0,\xi)}{\xi g(0,\xi,z)} d\xi = 0. \tag{2.4}$$

The relation $y=y_{\text{spk}}(z)$ defines a monotone decreasing curve in z (see Ref. 12). Let $(x_{\text{spk}}, y_{\text{spk}}, z)$ denote the intersection of the planar surface $y=y_{\text{spk}}(z)$ with $\mathcal{S}_a$, i.e., the projection of the curve $(0, y_{\text{spk}}(z), z)$ to the x-attracting nullcline $\mathcal{S}_a$ in the direction of x. Let $p_{\text{spk}} = (x_{\text{spk}}, y_{\text{spk}}, z_{\text{spk}})$ be the intersection of this curve with the curve γ as depicted in Fig. 1(b), see also Fig. 7 of Ref. 12. For points left of p_{spk} on the curve the vector fields are positive in y, and negative in y right of p_{spk}.

Conditions and mechanisms analyzed in our previous works are summarized in the text below and in Fig. 2.

Deng[13] proved that under the condition $z_{\text{spk}} < \bar{z}$, which defines a region of the original parameter space, a period-doubling cascade to chaos must take place as the nontrivial z-nullcline plane $y=y_f$ crosses the point p_{spk} from above for sufficiently small $0 < \varepsilon \ll 1$ and $\zeta = 0$. This scenario persists to some extent for sufficiently small $0 < \zeta \ll 1$. The cascade bifurcation is due to the existence of a junction-fold point,[20,21] at which the reduced vector field on the cylindrical parabola $\mathcal{S}_a$ for $\varepsilon > 0$ is tangent to the junction Pontryagin curve $(x_{\text{spk}}, y_{\text{spk}}, z)$. A similar junction-fold point will also appear later in our construction of the current chaos generating mechanism. As $y=y_f$ moves further up, the cascade turns into a period-1 cycle with little change in z but large swings in x and y.

The work of Ref. 14 demonstrated instead that the nontrivial equilibrium point p_f must become an unstable spiral if

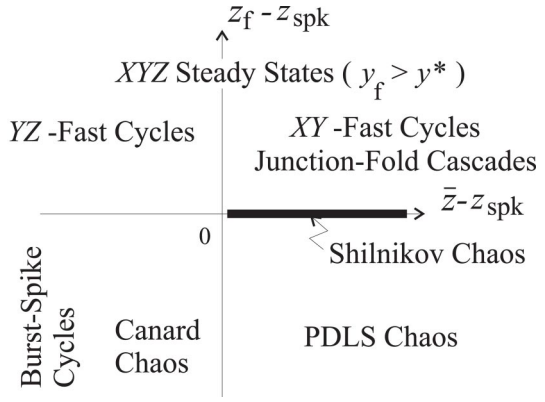

FIG. 2. Use $u := \bar{z} - z_{\text{spk}}$, $v := z_f - z_{\text{spk}}$ as new parameters. Then the various chaos generating mechanisms can be qualitatively summarized according to parameter partition in (u,v). This depiction holds for small $0 < \zeta \ll 1$, $0 < \varepsilon \ll 1$ except for the Shilnikov chaos case for which $\varepsilon \sim O(1)$. The result for the regions where yz-fast cycles, xyz steady states exist can be found in Ref. 12. The parameter region that is under consideration is the third uv-quadrant where the canard chaos and burst-spike cycles are found.

ε increases beyond a modest value ε_0. This occurs in another domain of the original parameter space. When coupled with the same condition that $z_{\text{spk}} < \bar{z}$, it was proven that at the point where p_f crosses p_{spk}, a singular Shilnikov saddle-focus homoclinic orbit[22] exists for $\zeta = 0$ and persists for all sufficiently small $0 < \zeta \ll 1$. Chaotic dynamics occurs as the result of such an orbit.

The work of Ref. 15 considered the same conditions as of Ref. 13 except that the nontrivial z-nullcline $y=y_f$ lies below the point p_{spk}: that is $z_f < z_{\text{spk}} < \bar{z}$. It was demonstrated that chaos occurs only because of the PDLS property of the y equation.

In this paper, we will consider the parameter region considered in Ref. 15 except that $\bar{z} \leqslant z_{\text{spk}}$, namely

$$0 < \bar{z} \leqslant z_{\text{spk}},\ z_f < z_{\text{spk}},\ 0 < \varepsilon \ll 1,\ 0 < \zeta \ll 1. \tag{2.5}$$

We will construct chaotic one-dimensional return maps for the system.

III. SINGULAR PERTURBATION

The dimensionless system (2.3) with singular parameters $0 < \varepsilon \ll 1, 0 < \zeta \ll 1$ permits a singular perturbation approach by which a full picture of the three-dimensional system can be constructed by piecing together lower dimensional systems at the singular limits when either $\zeta = 0$, $\varepsilon = 0$ or both.

Relaxation cycles: Consider Eq. (2.3) as a singularly perturbed system in $0 < \varepsilon \ll 1$ for which z is slowly varying. Setting $\varepsilon = 0$ gives rise to the ε-fast xy subsystem

$$\begin{aligned} \zeta\dot{x} &= xf(x,y) = x\left(1 - x - \frac{y}{\beta_1 + x}\right), \\ \dot{y} &= yg(x,y,z) = y\left(\frac{x}{\beta_1 + x} - \delta_1 - \frac{1}{\beta_2 + y}z\right), \\ \dot{z} &= 0, \end{aligned} \tag{3.1}$$

which is a family of two-dimensional systems in variables x and y with each z frozen as a parameter. The phase portrait

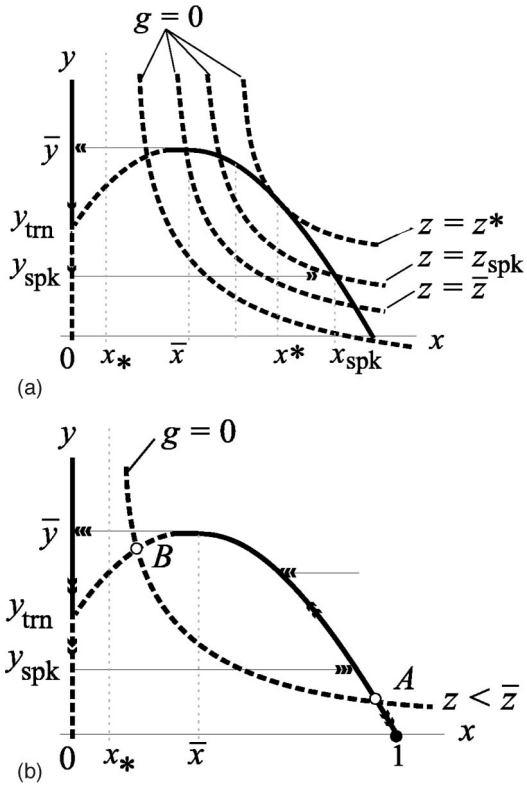

FIG. 3. Phase portraits of the ε-fast subsystem in x,y with $\zeta=0$. In (a) a few typical z-section curves of the nontrivial y-nullcline surface $g(x,y,z)=0$ are sketched together with the x-nullclines. For $z<\overline{z}$, the equilibrium point B is unstable and a singular limit cycle appears as shown in (b). For $z>\overline{z}$ but $z<z^*$, B is stable and the singular limit cycle is gone. For $z=\overline{z}$, B is a saddle-node point which interrupts the singular limit cycle. The equilibrium point A is always unstable. Both A and B coalesce when $z=z^*$ and disappear altogether for $z>z^*$. A three-dimensional view of these portraits stacked along the z axis is shown in Fig. 1(b).

for all fixed z can be easily constructed from the x and y nullclines. The Eq. (3.1) phase portraits are shown in Figs. 3(b) and 1(b). Figure 3(b) is for $0<z<\overline{z}$ for which the equilibrium point B is left of the fold-point $(\overline{x},\overline{y})$. It depicts the condition (2.5), $\overline{z}<z_{\rm spk}$, showing that the other equilibrium point A lies below the PDLS line $y=y_{\rm spk}$. For z from this region, the xy system has a singular limit cycle at $\zeta=0$ that starts at the fold and returns to itself by following the singular ζ-fast orbits parallel to the x axis and the singular ζ-slow orbits on the ζ-slow manifolds $x=0$ and $\mathcal{S}_a=\{f=0,f_x<0\}$. Singular limit cycles of this kind are referred to as full cycles in contrast to canard cycles which we will introduce later. All nonequilibrium singular orbits are attracted to either the full singular cycle or the steady state $(x,y)=(1,0)$ for $z<z_{\rm spk}$. The turning point $y_{\rm spk}$ is determined by the PDLS integral equation (2.4). For $0<\zeta\ll 1$ the full singular cycles persist in forms referred to as relaxation cycles.

Canard explosion: It is a singular perturbation phenomenon for a one-parameter family of two-dimensional systems. In our case, the singular perturbation parameter in question is $0<\zeta\ll 1$, the two-dimensional systems are the xy systems, and the parameter is z, corresponding to the other singular perturbation limit at $\varepsilon=0$. Under this setting, the point $\overline{p}=(\overline{x},\overline{y},\overline{z})$ with $z=\overline{z}$ for the xy equation is a nondegenerate canard point by definition because the following conditions are satisfied:

$$f(\overline{p})=0,\ \ g(\overline{p})=0,\ \ f_x(\overline{p})=0,$$

$$f_{xx}(\overline{p})\neq 0,\ \ f_y(\overline{p})\neq 0,\ \ g_x(\overline{p})\neq 0,\ \ g_z(\overline{p})\neq 0.$$

These conditions imply[23,24] that for small $0<\zeta\ll 1$ there must be a Hopf bifurcation point denoted by $\overline{p}(\zeta)$. Since we know for Eq. (3.1) a stable branch of equilibrium points arises from $\overline{p}$ for $z>\overline{z}$ along the curve γ, the Hopf bifurcation must be supercritical. According to the theory of nondegenerate canard points and in the notation of Ref. 24 the quantity A must be $A<0$ for our xy system, where $A<0$ iff the Hopf bifurcation is supercritical from a nondegenerate canard. Hence the results of Theorems 3.2, 3.3 of Ref. 24 should be applied to Eq. (3.1) although the latter theorem needs some modifications to account for singular cycles going through transcritical points rather than all fold points as assumed for the established theory. Hence, we will treat the description below as conjectured rather than proven. The conjectured will only be used in Theorem 4.2 of this paper.

The canard-Hopf periodic surface bifurcating from $\overline{p}(\zeta)$ can be continuously extended from the bifurcation point $\overline{z}(\zeta)$ to the lower endpoint $z=0$. Let Γ denote the surface. Then Γ can be effectively divided into two parts: $\Gamma=\Gamma_r\cup\Gamma_c$ for which Γ_r lies over an interval $0\leqslant z\leqslant z_r(\zeta)$ and Γ_c lies over the complement $[z_r(\zeta),\overline{z}(\zeta)]$. The left part Γ_r consists of xy periodic orbits of the relaxation type from full singular cycles [Fig. 3(b)], hence the subscript r stands for relaxation cycles. That is, for each $0\leqslant z\leqslant z_r$, the z-section of Γ_r is the unique relaxation cycle for the z-parametrized xy equation.

The description for Γ_c is slightly more complex. According to the theory[23,24] the following holds. Surface Γ_c can be further divided into two parts: $\Gamma_c=\Gamma_e\cup\Gamma_s$ for which Γ_e lies over an interval $[z_r(\zeta),z_s(\zeta)]$ and Γ_s lies over the complement $[z_s(\zeta),\overline{z}(\zeta)]$. The right part Γ_s consists of small periodic orbits bifurcating from the Hopf point $\overline{p}(\zeta)$, and is over a range of order $|z_s(\zeta)-\overline{z}(\zeta)|=O(\zeta)$. The subscript, s, of Γ_s stands for small cycles. The remaining part Γ_e over the interval $[z_r(\zeta),z_s(\zeta)]$ expands the surface from the small cycles to the relaxation full cycles, and the interval range is of an exponentially small order $|z_r(\zeta)-z_s(\zeta)|=O(e^{-1/\sqrt{\zeta}})$ [with ν of Ref. 24 to be fixed at $\nu=1/2$ as in the order estimate $O(e^{-1/\zeta^{1-\nu}})$].

The description above is fairly complete for the range of z as a parameter. More accurate description for the surface Γ, in particular, Γ_c goes as follows. For each $\nu\in(0,1)$ ($\nu=1/2$ in particular as above) and a small $\zeta_0>0$ both the frozen variable $z\in(z_r(\zeta),\overline{z}(\zeta))$ and the surface Γ_c can be parametrized by the singular parameter $\zeta\in(0,\zeta_0)$ and another auxiliary parameter $s\in(0,s_0)$ whose meaning will become apparent soon after. For now let $s_0:=2(\overline{y}-y_{\rm trn})$. That is, $z=z(\zeta,s),\Gamma_c=\Gamma_c(\zeta,s)$ for $\zeta\in(0,\zeta_0)$ and $s\in(0,s_0)$ and the parametrization is C^k smooth for any k. The parametrization means that for each fixed ζ from the interval, $z(\zeta,s)$ covers the range $(z_r(\zeta),\overline{z}(\zeta))$ as s ranges from s_0 to 0. According to the theory, $z(\zeta,s)$ is strictly decreasing in s for $s\in(0,\zeta^\nu)$ and $s\in(s_0-\zeta^\nu,s_0)$. For the fixed ζ, the corresponding periodic surface Γ_c is parametrized as $\Gamma_c(\zeta,s)$ in s as well. Most importantly, $\Gamma_c(\zeta,s)$ has a uniform limit as $\zeta\to 0$. As $\zeta\to 0$, the

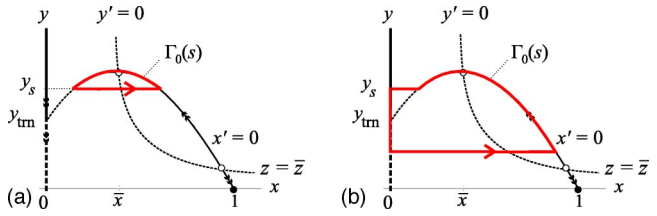

FIG. 4. (Color online). (a) An upside down limiting canard without a head for $0<s<\bar{y}-y_{\mathrm{trn}}$. (b) An upside down limiting canard with a square head for $\bar{y}-y_{\mathrm{trn}}<s<2(\bar{y}-y_{\mathrm{trn}})$. Both are depicted for $\zeta=0$.

canard explosion interval $[z_r(\zeta),\bar{z}(\zeta)]$ contracts to a point $\bar{z}(0)$. However, the limit $\Gamma_0(s):=\lim_{\zeta\to 0^+}\Gamma_c(\zeta,s)$ is still a family of cycles parametrized by s described below.

The parameter s that parametrizes both $\Gamma_c(\zeta,s)$ and its uniform limit $\Gamma_0(s)$ has a specific geometric interpretation. It defines a unique y value y_s at which singular solutions either jump right to the attracting cylindrical parabola x-nullcline $\mathcal{S}_a$ [Fig. 4(a)] or left to the attracting trivial x-nullcline $x=0$ [Fig. 4(b)]. More specifically, for $s=0$, $y_s=\bar{y}$ corresponds to the fold point, and for $0<s<\bar{y}-y_{\mathrm{trn}}$, $y_s=\bar{y}-s$, the y value s units below the fold $\bar{y}$. For $\bar{y}-y_{\mathrm{trn}}<s<2(\bar{y}-y_{\mathrm{trn}})$, $y_s=y_{\mathrm{trn}}+[s-(\bar{y}-y_{\mathrm{trn}})]$, the y value $s-(\bar{y}-y_{\mathrm{trn}})$ units above the transcritical point y_{trn}. As s continuously changes from 0 to $2(\bar{y}-y_{\mathrm{trn}})$, the singular orbit $\Gamma_0(s)$ continuously changes from canards without a head [Fig. 4(a)] to canards with a (square) head [Fig. 4(b)] and the point of transition takes place at the transcritical point y_{trn} at which $s=(\bar{y}-y_{\mathrm{trn}})$. To summarize, the singular limit of the periodic surface at $\zeta=0$ is the cylindrical limit cycle surface depicted in Fig. 1(b) open at both ends, $z=0$, $z=\bar{z}(0)$. It is not well defined at the right end $z=\bar{z}(0)$ because at this single z-section $z=\bar{z}(0)$ the surface limit takes up the family Γ_0 of all canard cycles with and without a head.

The most relevant property about canard explosion that we will use is the bifurcation curve in z with each fixed small $0<\zeta\ll 1$. Specifically, let Λ denote the intersection of the periodic surface Γ with $\mathcal{S}$ as shown in Figs. 1(a) and 5(c). Then the theory[23,24] predicts that Λ is a smooth curve having at least one local minimum in variable y. This is due to the fact that the PDLS curve on $\mathcal{S}$ is decreasing in y as z increases [see comment on (2.4)] and the fact that Λ traces tightly along the PDLS curve near $z=0$ and arises sharply near the canard point $\bar{p}$ due to the canard explosion. Most particularly, the limit of Λ at $\zeta=0$ consists of the vertical line $z=\bar{z}, y_{\mathrm{spk}}<y<\bar{y}$ and the Pontryagin return curve $(x_{\mathrm{spk}},y_{\mathrm{spk}},z)$, which is decreasing in y as z increases from 0 to $\bar{z}$, implying that $y_{\mathrm{spk}}(\bar{z})$ is the limiting absolute minimum. This conjectured curve Λ will be assumed for Theorem 4.2.

Pontryagin's delay of loss of stability: In Eq. (2.3), x evolves on the fastest time scale. In a perturbed state with $0<\zeta\ll 1$, all solutions are quickly attracted to a branch of the x-nullcline: either $\{x=0, y>\beta_1\}$ or $\mathcal{S}_a$ because the rate of change for x is much greater than that of y and z if their initial points are not already near these surfaces. In a sufficiently small neighborhood of the surfaces, solutions are well approximated by the reduced ζ-slow flows by setting $\zeta=0$ in Eq. (2.3),

$$xf(x,y)=0,\quad \dot{y}=yg(x,y,z),\quad \dot{z}=\varepsilon zh(y).$$

This is a two-dimensional system in y and z restricted to either $x=0$ or $\{f(x,y)=0\}$.

The yz dynamics is rather simple on $x=0$. In fact, the reduced yz equations are

$$\dot{y}=yg(0,y,z)=y\left(-\delta_1-\frac{1}{\beta_2+y}z\right)<0,$$

$$\dot{z}=\varepsilon zh(y)=\varepsilon z\left(\frac{y}{\beta_2+y}-\delta_2\right).$$

Hence all solutions develop downward towards $y=0$. They will cross the transcritical line $y=y_{\mathrm{trn}}=\beta_1$, at which $x=0$ loses its stability, and, in the sense of the asymptotic limit $\zeta=0$, jump to the stable branch of the nontrivial x-nullcline $f(x,y)=0$ at the delayed turning point $y=y_{\mathrm{spk}}(z)$.

The yz dynamics on the nontrivial and stable x-nullcline branch $\mathcal{S}_a$ is a little bit more complex, and determines the chaotic behavior we will describe later. Given $0\leqslant y\leqslant\bar{y}$, define $x=\psi(y):=\phi^{-1}(y)$ to be the value of x in $[\bar{x},1]$ such that (x,y) lies on the stable branch of $f(x,y)=0$; that is $f(\psi(y),y)=0$, $f_x(\psi(y),y)<0, 0\leqslant y\leqslant\bar{y}$. Then the reduced yz equations are

$$\begin{aligned}\dot{y}&=yg(\psi(y),y,z)=y\left(\frac{\psi(y)}{\beta_1+\psi(y)}-\delta_1-\frac{1}{\beta_2+y}z\right),\\ \dot{z}&=\varepsilon zh(y)=\varepsilon z\left(\frac{y}{\beta_2+y}-\delta_2\right).\end{aligned}\tag{3.2}$$

It is again a two-dimensional singularly perturbed system with singular parameter ε. The y equation is ε-fast, the z equation is ε-slow. Similar to the analysis for the ζ-fast xy subsystem (Refs. 13–15), the dynamics are essentially determined by the y-nullcline $\{y=0\}$, $\{g(x,y,z)=0\}$ and the z-nullcline $\{z=0\}$, $\{h(y)=0\}$. The two trivial nullclines, $\{y=0\}$ and $\{z=0\}$ are invariant and the dynamics on them are simple. The nontrivial y-nullcline restricted to $\mathcal{S}_a$ is the curve γ introduced earlier. The nontrivial z-nullcline $h(y)=0$ on $\mathcal{S}_a$ is $y=y_f=\beta_2\delta_2/(1-\delta_2)$. Two phase portraits are illustrated in Figs. 5(a) and 5(b). On the dashed part of the y-nullclines, the equilibria are repelling. On the solid portion, they are attracting. The ε-fast flows develop vertically and are shown with double arrows. Upon rescaling $t\to\varepsilon t$ and setting $\varepsilon=0$ in Eq. (3.2), it gives rise to the ε-slow subsystem in z restricted to the y-nullclines $y=0$ and γ. For points above the z-nullcline $y=y_f$, z increases on γ; and for points below it, z decreases on γ and $\{y=0\}$.

Most importantly, the point $(1,0,\underline{z})$ or $\underline{z}$ as shown in Fig. 5 is a transcritical point for Eq. (3.2) and the phenomenon of Pontryagin's delay of loss of stability occurs, now for the yz flow. The theory again applies. In particular, let (y,z) be any point from a fixed line, say $y=a$ with $0<a<y_f$. The perturbed flow [with $0<\varepsilon\ll 1$ in Eq. (3.2)] through (y,z) moves down and to the left, following the vector field. It crosses γ horizontally and then moves up and still left until hitting the line $y=a$ again at a point denoted by $(a,w_\varepsilon(z))$. This defines

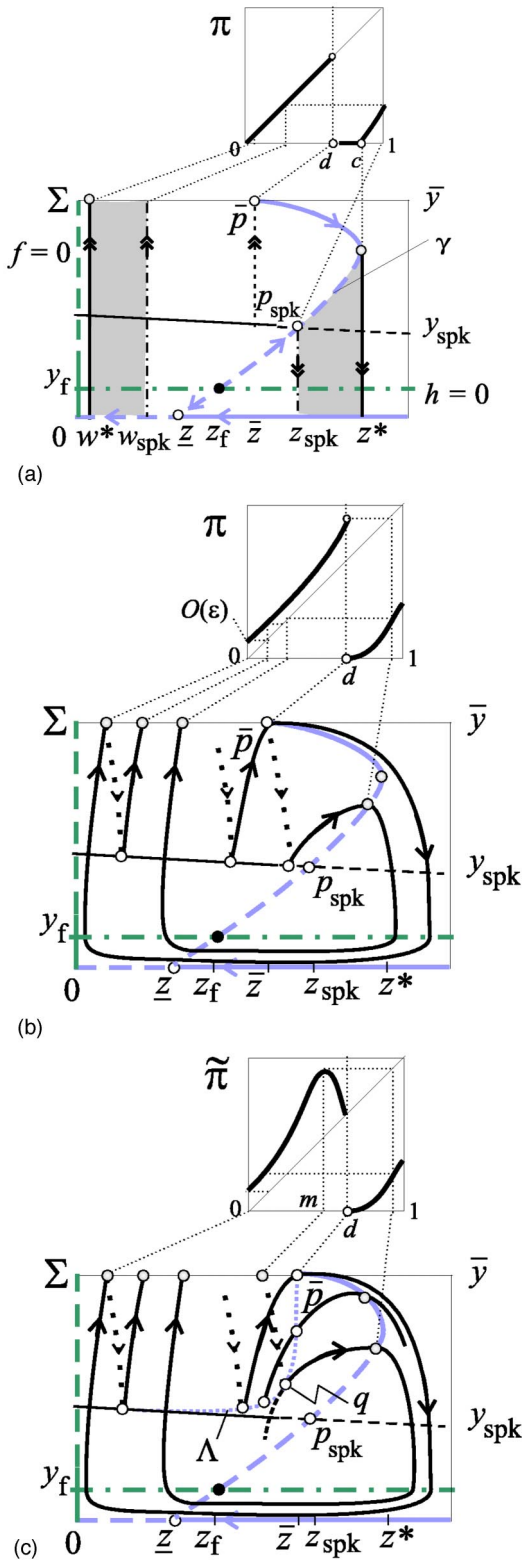

FIG. 5. (Color online). Phase portraits of the yz subsystems on the stable branch of the nontrivial x-nullcline $\mathcal{S}_a$ and the corresponding singular return maps for $\zeta=0$ in (a) and (b) and an approximating return map for $0<\zeta\ll 1$ in (c). (a) The case with $\zeta=\varepsilon=0$. The ε-fast flows develop vertically and are shown with double arrows. The oriented parts of the y-nullcline with a single arrow are the reduced ε-slow flow lines. (b) The return map at the perturbed state $0<\varepsilon\ll 1$. Dotted curves with a single arrow are the yz flow lines on the trivial x-nullcline $x=0$. (c) The same as (b) except that the canard explosion curve Λ is included on which the point q is a junction fold point. Unlike (a),(b), the map $\tilde{\pi}$ is a conjectured approximating map for $\zeta>0$. See text for description.

a diffeomorphism from z to $w_\varepsilon(z)$. Pontryagin's theory implies that $\lim_{\varepsilon\to 0} w_\varepsilon(z)=w(z)$ exists and $w(z)$ is determined by the following integral:

$$\int_z^w \frac{g(1,0,s)}{sh(0)}ds=0. \tag{3.3}$$

By simplifying the integral equation, we find that z and w satisfy the equation $z\exp(-z/\underline{z})=w\exp(-w/\underline{z})$. Because the function $y=x\exp(-x/\underline{z})$ increases in $(0,\underline{z}]$ and decreases in $[\underline{z},\infty)$, covering the same range $(0,\underline{z}/e]$, the correspondence between z and w is diffeomorphic. In particular, if we consider the shaded region in Fig. 5(a), also Fig. 1(b), bounded by points z_{spk} and z^*, then each vertical segment of the flow in this region corresponds to a unique vertical flow segment in the shaded region bounded by w^* and w_{spk}. This pair of vertical segments together with the ε-slow horizontal flow line from z to w along $\{x=1,y=0\}$ form the singular orbit for an initial condition below the γ curve.

Junction fold point: Recall the canard explosion curve Λ. With respect to the ζ-slow yz flow of Eq. (3.2) for $0<\varepsilon\ll 1$, the reduced yz vector field points up on Λ at points near $z=0$ far away from $z=\bar{z}$, and points right horizontally at the canard-Hopf point $\bar{p}$. That is, the vector field points at opposite side of the curve Λ near its two ends. Since the reduced yz vector field varies continuously along Λ, there must be a point at which the vector field is tangent to Λ, pointing to neither sides of Λ. Because Λ is parabolalike near $\bar{p}$ due to the Hopf bifurcation, there must be such a point, q, that the curve Λ lies locally to the left of the reduced yz vector field at q, see Fig. 5(c). By definition, such a point q is a junction-fold point.[13] The single most important property of the junction-fold point q that will be used later is that the yz solution curves starting on Λ below q will intersect Λ above q. Namely, solutions starting on both sides of q on Λ will overlap on each other as they move forward in time, a property that always gives rise to a fold point of the yz flow induced one-dimensional connecting or return map.[13,20,21,25] We will develop this construction further in the section below.

IV. RETURN MAPS AND CHAOS

We now describe the Poincaré return maps induced first by singular orbits of the full system Eq. (2.3) for $\zeta=0$, $0\leqslant\varepsilon\ll 1$ and then by approximating orbits for $0<\zeta\ll 1$, $0<\varepsilon\ll 1$.

Recall the periodic surface Γ that arises from the canard-Hopf point $\bar{p}$. It must intersect the y-nullcline $g(x,y,z)=0$ along a parabolalike curve. The upper half of the curve represents points at which orbits of the full system reach local maximum values in their y component, whereas the lower half of the curve represents points at which orbits reach local minima in y. Similarly, the reduced yz orbits on the surface $\mathcal{S}_a$ for $\zeta=0$ reach local maxima in y on the segment of curve γ over the interval $y_f\leqslant y\leqslant\bar{y}$. The curve γ persists for small $0<\zeta\ll 1$ for the ε-fast xy system as the fixed point branch bifurcating from the canard-Hopf point $\bar{p}$.

To define the return maps, let their domains of definition be the upper half of the intersection of the periodic surface Γ

with $g=0$ together with the segment of γ over the interval $y_{\text{spk}} \leqslant y \leqslant \overline{y}(\zeta)$, where $y_f < y_{\text{spk}}$ by condition (2.5). In other words, the maps are defined whenever orbits reach local maximum in the y coordinate. At the singular limit $\zeta=0$, we can simply let Σ be the union of the fold line $x=\overline{x}$, $y=\overline{y}$, $0 \leqslant z \leqslant \overline{z}$ and $\gamma \cap \{y_{\text{spk}} \leqslant y \leqslant \overline{y}\}$ and define the Poincaré return maps from Σ, see Figs. 1(b), 5(a), and 5(b). Such maps are equivalent to the ones through the local y-maximum curve on Γ and $\mathcal{S}$. In fact, the upper half of $\Gamma \cap \{g=0\}$ lies on the x-fast orbits initiated from the fold Σ as shown in Fig. 1(b). We parametrize points on Σ in terms of their arc length from the left most point of returning points of Σ. We further normalize Σ against its total length, and denote thus normalized return maps by π on the unit interval [0, 1] with $s \in [0,1]$ being the normalized arc length. With this setup we now describe below the return maps for three cases: $\zeta=0$, $\varepsilon=0$; respectively, $\zeta=0$, $\varepsilon>0$; and $\zeta>0$, $\varepsilon>0$. As mentioned earlier, we will only use the conjectured result on canard explosion for the third case.

One effective way to view the return map is to look directly into the x axis as shown in Fig. 5. The solid oriented curves are the ζ-slow orbits on the attracting branch of the cylindrical parabola $\mathcal{S}_a$. The dotted, downward-oriented curves are those on the trivial x-nullcline $x=0$ for $y \geqslant y_{\text{spk}}$. The fast jumps from the fold to the plane $x=0$ as well as from the Pontryagin turning curve $y=y_{\text{spk}}$ to $\mathcal{S}_a$ are perpendicular to the projected yz plane, and thus are hidden from the view.

The case of $\zeta=\varepsilon=0$ is relatively simple. The y-fold point p^* on Σ returns to Σ at $(\overline{x},\overline{y},w^*)$ as the left most point of π's range, see Fig. 5(a). Hence we set its normalized arc length at $(\overline{x},\overline{y},w^*)$ as 0. The normalized arc length for point p_{spk} is thus 1. Every point from $w^* < z < \overline{z}$ returns to itself, and therefore the graph of the π lies on the diagonal. For points from γ between $\overline{p}$ and p^*, they all return to the same left most point w^* or 0 on the interval [0, 1]. Because of Pontryagin's delay of loss of stability, the γ segment between p^* and p_{spk} returns diffeomorphically to an interval. The return of the canard point is not defined since it can be either considered as following the x-fast orbit first and then returning to itself, or following the z-slow orbit first on γ and then return to 0. We denote by $d=\pi(d^-)$ the former situation and by $0=\pi(d^+)$ the latter situation.

The case of $\zeta=0$, $\varepsilon>0$ is the same as the previous case except that we need to add rightward drift to orbits when they move above the z-nullcline $y=y_f$ and leftward drift when they move below $y=y_f$. Since we assume $\overline{z} < z_{\text{spk}}$, the return of the left limit $\pi(d^-)$ should be the maximum of π for sufficiently small $\varepsilon>0$ as shown in Fig. 5(b) and the return of the right limit $\pi(d^+)$ is the minimum point 0. If $\pi^2(d^-) > \pi^2(0)$, then the same proof of Ref. 15 can be used to prove that π contains subdynamics that is equivalent to a chaotic subshift map on two symbols. The condition that $\pi^2(d^-) > \pi^2(0)$ must hold by first choosing small $\varepsilon>0$ so that $\pi^2(0)=O(\varepsilon) < \pi(1)=O(1)$ and then pushing $\overline{p}$ rightward if necessary so that $\pi^2(d^-)$ is near $\pi(1)$. Hence we have proved the following result.

Theorem 4.1: *For $\zeta=0$ and sufficiently small $0<\varepsilon\ll 1$, there is a range of $\overline{z} < z_{\text{spk}}$ and $z_f < z_{\text{spk}}$ so that the singular Poincaré return map π has a subdynamics that is equivalent to a chaotic subshift map on two symbols.*

Conditions for the existence of attracting periodic orbits can also be stated for the return map. Let $I_r=[d,\pi(d^-)]$. If the critical point d is not in the k-iteration $\pi^k(I_r)$ where k is the first integer such that $\pi^k(I_r) \subset [0,d)$ and $\pi^{k+1}(I_r) \subset (d,1]$ and if $\pi(I_r) \subset [0,\pi(0)]$, then it is easy to show that the ω-limit set $\lim_{k\to\infty} \pi^k(I_r)$ contains stable periodic orbits only. Corresponding conditions for the full system are hard to prescribe. Intuitively, separating $\overline{z}$ and z_{spk} further apart is likely to make $\pi^2(d^-)$ smaller relative to $\pi(0)$ because the PDLS effect near the point p_{spk} will be diminished.

The case of $\zeta>0$, $\varepsilon>0$ is slightly more complicated, mainly because it involves the full ramification of canard explosion. In this case the full dynamics of Eq. (2.3) is three-dimensional and any return map must be two-dimensional on the surface when y is local maximum. For sufficiently small $0<\zeta\ll 1$ all solutions are well-approximated by solutions on $\mathcal{S}_a$ whenever they are nearby. Hence such a two-dimensional return map has a good one-dimensional approximation. More specifically, the canard-Hopf periodic surface Γ is attracting and part of it is near $\mathcal{S}_a$. Thus we can use solutions on the surfaces Γ and $\mathcal{S}_a$ as approximating flows. Now an approximating map, $\tilde{\pi}$ depicted in Fig. 5(c), is defined as follows. For points left the prepoint of the canard-Hopf point $\overline{p}$ on Σ, we follow them around the surface Γ, connect them to the curve Λ, and then return them *on* Γ to Σ. For points right of the prepoint and left of $\overline{p}$, we follow them around the surface Γ, connect them to the curve Λ first, follow them on Γ to Λ again, then return them *on* $\mathcal{S}_a$ to $\gamma \subset \Sigma$. For points right of $\overline{p}$, we follow the flows from γ on $\mathcal{S}_a$ around p_f and then *on* Γ before returning them to Σ. Note that this map is a hybrid of $\zeta=0$ flows on $\mathcal{S}_a$ and flows on the bifurcation surface Γ defined for $\zeta>0$. Also note that the prepoint on Σ for the junction-fold point q is a global maximum for $\tilde{\pi}$ at which $\tilde{\pi}'=0$. Except for the additional features that it is decreasing over the interval $[m,d)$ and $\tilde{\pi}'(m)=0$, the map $\tilde{\pi}$ behaves similarly as the return map π from the previous case for $\zeta=0$, $\varepsilon>0$. Similar result as Theorem 4.1 applies.

Theorem 4.2: *Assume the existence of the canard explosion curve Λ for sufficiently small $0<\zeta\ll 1$. Then there exists a range of $0<\varepsilon\ll 1$, $\overline{z} < z_{\text{spk}}$, and $z_f < z_{\text{spk}}$ so that the hybrid return map $\tilde{\pi}$ has a subdynamics that is equivalent to a chaotic subshift map on two symbols.*

For a set of parameter values satisfying (2.5), a chaotic tea-cup attractor together with its return map through the local maximum surface $\dot{y}=0$ are shown in Fig. 6. A junction-fold point is marked as q on Fig. 6(a) and our hybrid return map, Fig. 5(c), matches well with the numerical return map, Fig. 6(b), which in theory is two dimensional.

V. CLOSING REMARKS

We have given a mechanistic singular perturbation explanation to some chaotic and periodic attractors of the tea-cup type in the Rosenzweig–MacArthur food chain model. We demonstrated that although canard singularity is key to the tea-cup feature it alone does not lead to chaos, unlike the other three mechanisms analyzed in Refs. 13–15. We dem-

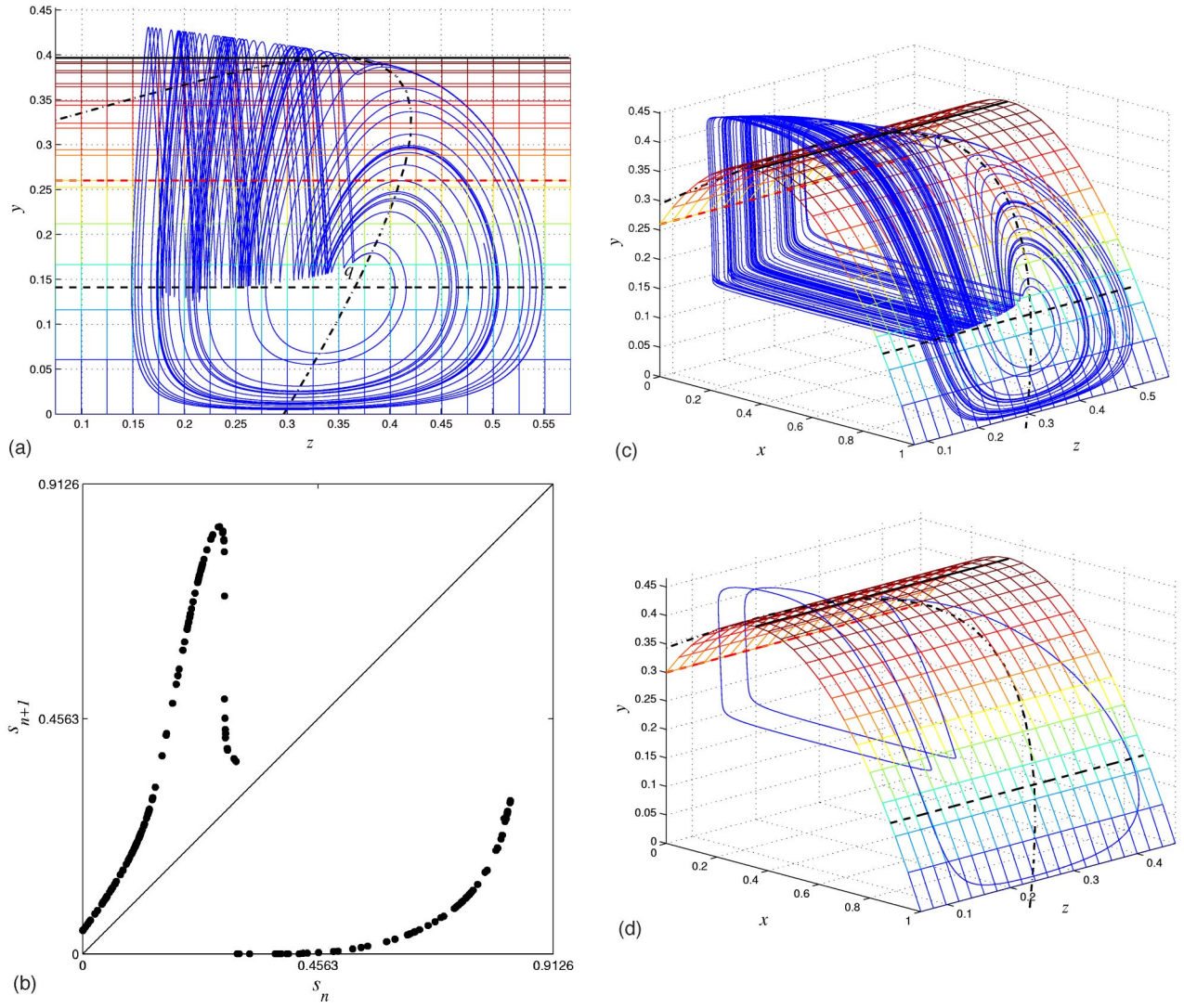

FIG. 6. (Color online). Numerical simulations with parameter values $\zeta=0.02$, $\varepsilon=0.24$, $\beta_1=0.26$, $\beta_2=0.5$, $\delta_1=0.2$, $\delta_2=0.22$ for (a), (b), and (c) and the same values except for $\beta_1=\delta_1=0.3$ for (d). (a) The yz projection view. (b) The Poincaré return map through the local y-maximum surface and points are parametrized by arc length s. (c) A three-dimensional view. (d) A periodic orbit as the $\bar{z}$ moves farther away from z_{spk} as predicted by our analysis.

onstrated instead that the chaotic behavior is largely due to the PDLS phenomenon of the predator dynamics. However, because of the canard point, techniques to construct singular return maps from our previous works cannot be directly applied. Instead we had to use predator's local maximum surface $\dot{y}=0$ as the cross section for the return map construction. In addition, unlike the other cases where all return maps arise from direct singular limits, a hybrid return map, which makes use of both limiting and perturbed structures of the system, is used to approximate the junction-fold effect from the canard explosion. Comparing to the other three types of food chain chaos, the tea-cup attractors are better known, more complex, and harder to analyze. In the end its key ingredient plays a less prominent role than its simpler counterparts—the junction-fold point and the transcritical point.

The chaotic structures categorized by the series of Refs. 13–15 and this paper are closely related to the bursting and spiking phenomena found in models for neurons and excitable membranes, cf. Refs. 26–31. A proof of chaotic dynamics for the latter was first given in Ref. 30 using a two-time-scale singular perturbation analysis, and a proof of a period-doubling cascade to chaos was given in Ref. 21 using a three-time-scale singular perturbation analysis. The behavioral similarity between these two types of models was first alluded to in Ref. 9. The current approach by a three-time-scale singular perturbation analysis was first adopted in Refs. 12 and 11 for food chains and concurrently in Ref. 32 for excitable membranes. The proof of food chain chaos from Ref. 13 has since united these two areas within the same framework of three-time-scale singular perturbation analysis. We envision that a variety of chaos generating mechanisms for neuron models should be systematically categorized and analyzed by the same methodology.

APPENDIX: EXISTENCE OF *Y*-FOLD

Proposition 6.1: Under conditions

$$\bar{x}=\frac{1-\beta_1}{2}<\frac{\beta_1\delta_1}{1-\delta_1}=x_*$$

and $\beta_2 < \dfrac{(\beta_1+1)^3}{\beta_1}\left(\dfrac{1}{\beta_1+1}-\delta_1\right)$

there is a unique y-fold point (x^*,y^*,z^*) *at which the y-nullcline curve* $\gamma=\{f(x,y)=0, f_x(x,y)<0\}\cap\{g(x,y,z)=0\}$ *on* $\mathcal{S}_a$ *reaches its maximum in the z variable.*

Proof: Solve z from $g(x,y,z)=0$ as $z=P(x,y)=[(x/\beta_1+x)-\delta_1](\beta_2+y)$ and $x=\phi^{-1}(y)$ with $\phi(x)=(1+x)(\beta_1+x)$ from $f(x,y)=0$, $f_x(x,y)<0$ for $\overline{x}<x<1$ and $0<y<\overline{y}$. Then γ can be expressed as $z=p(y)=P(\phi^{-1}(y),y)$ for $0<y<\overline{y}$. The idea is to show that $z_y=p'(y)$ has a unique zero by showing $p'(0)>0$, $p'(\overline{y})<0$ and that p is decreasing.

With $x=\phi^{-1}(y)$ below we have

$$
\begin{aligned}
z_y = p'(y) &= \frac{\beta_1}{(\beta_1+x)^2}(\phi^{-1})'(y)(\beta_2+y)+\left(\frac{x}{\beta_1+x}-\delta_1\right)=\frac{\beta_1}{(\beta_1+x)^2}\left(-\frac{f_y}{f_x}\right)(\beta_2+y)+\left(\frac{x}{\beta_1+x}-\delta_1\right)\\
&=\left(-\frac{f_y(\beta_1+x)}{f_x}\right)\left[\frac{\beta_1}{(\beta_1+x)^3}(\beta_2+y)+\left(-\frac{f_x}{f_y(\beta_1+x)}\right)\left(\frac{x}{\beta_1+x}-\delta_1\right)\right]\\
&=\frac{1}{f_x}\left[\frac{\beta_1}{(\beta_1+x)^3}(\beta_2+y)+f_x\left(\frac{x}{\beta_1+x}-\delta_1\right)\right]\quad\left(\text{since } f_y=-\frac{1}{\beta_1+x}\right).
\end{aligned}
$$

Since $f_x=-1+[y/(\beta_1+x)^2]=-1$ at $y=0$, $x=\underline{x}=1$, we have immediately

$$
\begin{aligned}
z_y|_{\{x=1,y=0\}} &= -\left[\frac{\beta_1\beta_2}{(\beta_1+1)^3}-\left(\frac{1}{\beta_1+1}-\delta_1\right)\right]\\
&=-\frac{\beta_1}{(\beta_1+1)^3}\left[\beta_2-\frac{(\beta_1+1)^3}{\beta_1}\times\left(\frac{1}{\beta_1+1}-\delta_1\right)\right]>0
\end{aligned}
$$

by the assumption on β_2. Also, as $y\to\overline{y}^-$, $x\to\overline{x}^+$, and $f_x\to 0^-$. Therefore,

$$
z_y|_{\{y\to\overline{y}^-\}}=\lim_{y\to\overline{y}^-}\left\{\left(\frac{1}{f_x}\right)\left[\frac{\beta_1}{(\beta_1+x)^3}(\beta_2+y)+f_x\left(\frac{x}{\beta_1+x}-\delta_1\right)\right]\right\}=-\infty.
$$

Therefore there must be a zero of $z_y=p(y)$ between $y=0$ and $y=\overline{y}$. So it is only left to show that the zero is unique.

To this end, rewrite with the knowledge that $y=\phi(x)$,

$$
z_y=\frac{1}{f_x}\left[\frac{\beta_1}{(\beta_1+x)^3}(\beta_2+y)+f_x\left(\frac{x}{\beta_1+x}-\delta_1\right)\right]:=\frac{1}{f_x}Q(x).
$$

Then we know $Q(1)<0$, $Q(\overline{x})>0$, and we only need to show $Q'(x)<0$ for $x\in(\overline{x},1]$. Writing Q as

$$
Q(x)=\frac{\beta_1}{(\beta_1+x)^3}(\beta_2+y)+\left(-1+\frac{y}{(\beta_1+x)^2}\right)\times\left(\frac{x}{\beta_1+x}-\delta_1\right)
$$

we see that $Q'(x)<0$. In fact, the first term is obviously decreasing in x. The second term is the product of two factors: $a(x)b(x):=f_x\{[x/(\beta_1+x)]-\delta_1\}$. By the product rule, we have $a'(x)b(x)+a(x)b'(x)$. Since $a=f_x$ is negative, decreasing, and b is increasing and positive since $x>\overline{x}=(1-\beta_1)/2>x_*=\beta_1\delta_1/(1-\delta_1)$ and $x_*/(\beta_1+x_*)-\delta_1=0$, we see clearly that it is decreasing for the product. This completes the proof. □

[1] R. May, "Simple mathematical models with very complicated dynamics," Nature (London) **261**, 459–467 (1976).
[2] P. Hogeweg and B. Hesper, "Interactive instruction on population interactions," Comput. Biol. Med. **8**, 319–327 (1978).
[3] M.E. Gilpin, "Spiral chaos in a predator-prey model," Am. Nat. **113**, 306–308 (1979).
[4] O.E. Rössler, "Chaotic behavior in simple reaction systems," Z. Naturforsch. A **31A**, 259–264 (1976).
[5] A. Hastings and T. Powell, "Chaos in a three-species food chain," Ecology **72**, 896–903 (1991).
[6] L.P. Šil'nikov, "A case of the existence of a denumerable set of periodic motions," Sov. Math. Dokl. **6**, 163–166 (1965).
[7] K. McCann and P. Yodzis, "Bifurcation structure of a three-species food chain model," Theor Popul. Biol. **48**, 93–125 (1995).
[8] H.L. Smith and P. Waltman, *The Theory of the Chemostat—Dynamics of Microbial Competition*, Cambridge Studies in Mathematical Biology (Cambridge University Press, Cambridge, 1994).
[9] Yu.A. Kuznetsov and S. Rinaldi, "Remarks on food chain dynamics," Math. Biosci. **133**, 1–33 (1996).
[10] M.L. Rosenzweig and R.H. MacArthur, "Graphical representation and stability conditions of predator-prey interactions," Am. Nat. **97**, 209–223 (1963).
[11] S. Rinaldi and S. Muratori, "Slow-fast limit cycles in predator-prey models," Ecol. Modell. **61**, 287–308 (1992).
[12] S. Muratori and S. Rinaldi, "Low- and high-frequency oscillations in three-dimensional food chain system," SIAM (Soc. Ind. Appl. Math.) J. Appl. Math. **52**, 1688–1706 (1992).
[13] B. Deng, "Food chain chaos due to junction-fold point," Chaos **11**, 514–525 (2001).
[14] B. Deng and G. Hines, "Food chain chaos due to Shilnikov orbit," Chaos **12**, 533–538 (2002).
[15] B. Deng and G. Hines, "Food chain chaos due to transcritical point," Chaos **13**, 578–585 (2003).
[16] C.S. Holling, "Some characteristics of simple types of predation and parasitism," Canadian Entomologist **91**, 385–398 (1959).
[17] L.C. Pontryagin, "Asymptotic behavior of solutions of systems of differential equations with a small parameter at higher derivatives," Izv. Akad. Nauk SSSR, Ser. Mat. **21**, 605–626 (1957).
[18] E.F. Mishchenko, Yu.S. Kolesov, A.Yu. Kolesov, and N.Kh. Rozov, *Asymptotic Methods in Singularly Perturbed Systems*, Monographs in

Contemporary Mathematics (Consultants Bureau, New York, 1994).
[19]S. Schecter, "Persistent unstable equilibria and closed orbits of a singularly perturbed equation," J. Diff. Eqns. **60**, 131–141 (1985).
[20]B. Deng, "Folding at the genesis of chaos," in *Proceedings of the First World Congress of Nonlinear Analysts* (Walter de Gruyter, Berlin, 1996), Vol. IV, pp. 3765–3777.
[21]B. Deng, "Glucose-induced period-doubling cascade in the electrical activity of pancreatic β-cells," J. Math. Biol. **38**, 21–78 (1999).
[22]K. Taylor and B. Deng, "Chaotic attractors in one-dimension generated by a singular Shilnikov orbit," Int. J. Bifurcation Chaos Appl. Sci. Eng. **12**, 3059–3083 (2001).
[23]F. Dumortier and R. Roussarie, *Canard Cycles and Center Manifolds*, Memoirs of the American Mathematical Society, Vol. 577 (American Mathematical Society, Providence, RI, 1996).
[24]M. Krupa and P. Szmolyan, "Relaxation oscillation and canard explosion," J. Diff. Eqns. **174**, 312–368 (2001).
[25]B. Deng, "Constructing homoclinic orbits and chaotic attractors," Int. J. Bifurcation Chaos Appl. Sci. Eng. **4**, 823–841 (1994).
[26]T.R. Chay and J. Keizer, "Minimal model for membrane oscillations in the pancreatic β-cell," Biophys. J. **42**, 181–190 (1983).
[27]T.R. Chay, "Chaos in a three-variable model of an excitable cell," Physica D **16**, 233–242 (1985).
[28]T.R. Chay and J. Rinzel, "Bursting, beating, and chaos in an excitable membrane model," Biophys. J. **47**, 357–366 (1985).
[29]J. Rinzel, "Bursting oscillations in an excitable membrane model," in *Ordinary and Partial Differential Equations*, edited by B.D. Sleeman and R.J. Jarvis (Springer, New York, 1985), pp. 304–316.
[30]D. Terman, "Chaotic spikes arising from a model of bursting in excitable membranes," SIAM (Soc. Ind. Appl. Math.) J. Appl. Math. **51**, 1418–1450 (1991).
[31]E.M. Izhikevich, "Neural excitability, spiking and bursting," Int. J. Bifurcation Chaos Appl. Sci. Eng. **10**, 1171–1266 (2000).
[32]B. Deng, "A mathematical model that mimics the bursting oscillations in pancreatic β-cells," Math. Biosci. **119**, 241–250 (1993).